JOURNAL OF GEOPHYSICAL RESEARCH, VOL. 108, NO. C4, 3122, doi:10.1029/2002JC001508, 2003

Seasonal, interannual, and mesoscale variability of the Black Sea upper layer circulation derived from altimeter data

Gennady Korotaev,[1] T. Oguz,[2] A. Nikiforov,[1] and C. Koblinsky[3]

Received 11 June 2002; revised 5 December 2002; accepted 30 January 2003; published 19 April 2003.

[1] TOPEX/Poseidon and ERS altimeter data comprising the period from May 1992 to May 1999 are assimilated into a shallow water model for providing a dynamically consistent interpretation of the sea surface height variations and estimation of the temporal and spatial characteristics of the upper layer circulation in the Black Sea. These 7-year-long observations offer a new capability for interpretation of major transient and quasi-permanent features of the upper layer circulation. The instantaneous flow fields involve a complex, eddy-dominated system with different types of structural organizations in which the eddies and the gyres of the interior cyclonic cell interact continuously among themselves and with meanders, and filaments of the Rim Current. The circulation possesses a distinct seasonal cycle whose major characteristic features repeat every year with some year-to-year variability. An organized two-gyre winter circulation system disintegrates gradually into a series of interconnecting eddies in the summer and autumn months, which are also characterized by more pronounced and complex mesoscale activity in the peripheral flow system. Our analyses suggest a revised schematic circulation picture of the major quasi-permanent and recurrent elements of the Black Sea. *INDEX TERMS:* 4243 Oceanography: General: Marginal and semienclosed seas; 4512 Oceanography: Physical: Currents; 4520 Oceanography: Physical: Eddies and mesoscale processes; 4556 Oceanography: Physical: Sea level variations; *KEYWORDS:* Black Sea, circulation, sea level variation, altimeter data, data assimilation

Citation: Korotaev, G., T. Oguz, A. Nikiforov, and C. Koblinsky, Seasonal, interannual, and mesoscale variability of the Black Sea upper layer circulation derived from altimeter data, *J. Geophys. Res.*, *108*(C4), 3122, doi:10.1029/2002JC001508, 2003.

1. Introduction

[2] Understanding of the Black Sea circulation has significantly increased during the last decade through realization of several international programs. Compared to earlier findings from coarse resolution hydrographic data [e.g., *Blatov et al.*, 1984; *Simonov and Altman*, 1991], circulation inferred from the recent medium-resolution, quasi-synoptic, multiship field surveys [*Oguz et al.*, 1993, 1994; *Krivosheya et al.*, 1998; *Oguz and Besiktepe*, 1999; *Gawarkiewicz et al.*, 1999; *Besiktepe et al.*, 2001; *Sokolova et al.*, 2001], and satellite data [*Oguz et al.*, 1992; *Grishin*, 1994; *Sur et al.*, 1994, 1996; *Ginsburg et al.*, 2000; *Stanev et al.*, 2000; *Korotaev, et al.*, 2001; *Sokolova et al.*, 2001; *Oguz et al.*, 2002] involves ubiquitous mesoscale structures superimposed on its basin and subbasin-scale elements. Analyzing all the available data, *Oguz et al.* [1993] specified the building blocks of the upper layer circulation as (1) the Rim Current system around the periphery, (2) an interior cell composed by two or more cyclonic gyres, and (3) a series of quasi-stable/recurrent anticyclonic eddies on the coastal side of the Rim Current (Figure 1). Superimposed on this pattern, the instantaneous circulation contains seemingly transient mesoscale activity in the form of meanders of the Rim Current jet and mesoscale eddies on both sides. However, limited time series of clear sky scenes in AVHRR and SeaWiFS images do not allow the monitoring of the evolution of distinct circulation features and to distinguish firmly how and when the quasi-permanent eddies differ from transient ones.

[3] Construction of optimally interpolated and gridded (in both space and time) dynamical sea level data from altimetry [*Korotaev et al.*, 2001] recently provided a new resource for increasing our present level of knowledge on variability of the Black Sea circulation. They described the methodology for reconstruction of the dynamical sea level data base for the period from May 1992 to November 1996, its validation by the available hydrographic survey data, and interpretation of the results by means of a simple two-layer analytical model of the wind-driven circulation in a rectangular basin. Using five years of TOPEX/Poseidon (hereinafter referred to as T/P) data, *Ducet et al.* [1999] dealt with the application of atmospheric pressure correction to the Black Sea mean level, and analyzed the response of the mean sea level to wind forcing in relation with the exchange through the Bosphorus Strait. *Stanev et al.* [2000] and *Sokolova et al.* [2001], utilizing combination of the T/P altimeter, hydrological and meteorological data, investigated properties of the basin integrated water balance and determined a time series estimate of the net outflow through

[1]Marine Hydrophysical Institute, National Academy of Sciences of Ukraine, Sevastopol, Ukraine.
[2]Institute of Marine Sciences, Middle East Technical University, Erdemli, Turkey.
[3]NASA Goddard Space Flight Center, Greenbelt, Maryland, USA.

0148-0227/03/2002JC001508$09.00

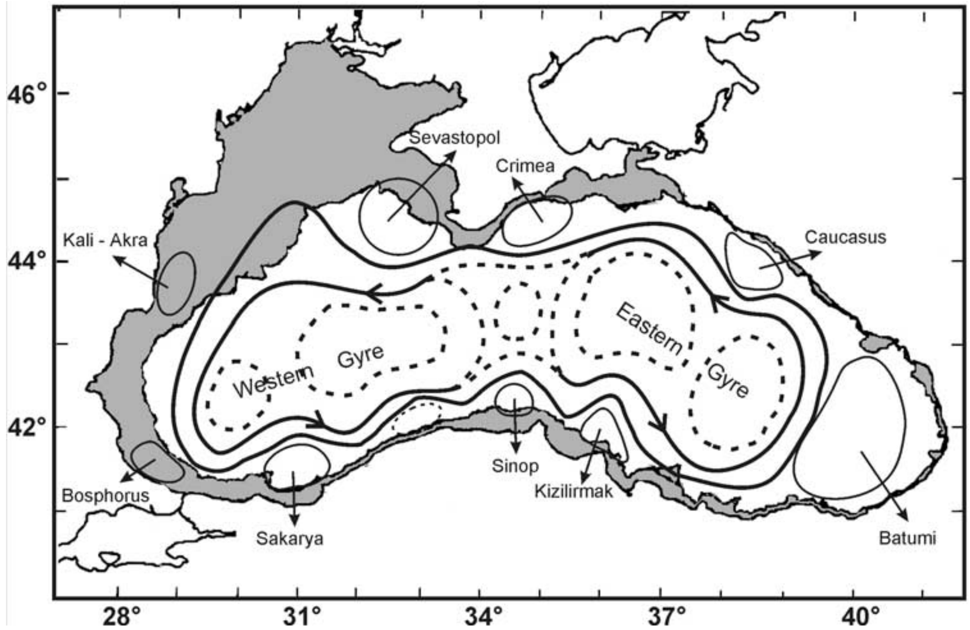

Figure 1. The schematic diagram for the main features of the upper layer circulation derived from synthesis of past hydrographic studies prior to 1990 (reproduced from its original given by *Oguz et al.* [1993]).

the Bosphorus Strait. Moreover, they identified predominant features of the circulation at intraannual, seasonal and interannual timescales. These variations have been related to westward Rossby wave propogation superimposed on oscillations induced by direct wind forcing.

[4] The present paper complements these former studies and describes the upper layer circulation of the Black Sea by way of assimilating altimeter data into a simple, 1.5 layer, shallow-water model. The altimeter data considered in this work involve a combination of the 7-year-long T/P and ERS-I, II sea level measurements encompassing the period from May 1992 to May 1999. This combined data set provides much finer spatial coverage of the altimeter observations (see Figure 2 for the typical T/P and ERS tracks) with respect to those based on only the T/P measurements [*Stanev et al.*, 2000; *Sokolova et al.*, 2001], and with respect to the ERS-I data covered only until the end of 1993 [*Korotaev et al.*, 1999]. An outline of the data processing and dynamical sea level construction methodologies are presented in section 2. Following a brief description of the data assimilation approach in section 3, section 4 explores characteristics of the wind-driven circulation in the absence of altimeter data assimilation. Section 5 extends these results to the case of model simulations with data assimilation, and concentrates specifically on seasonal, interannual and climatological mean (i.e., the average of the 7 years of data coverage)

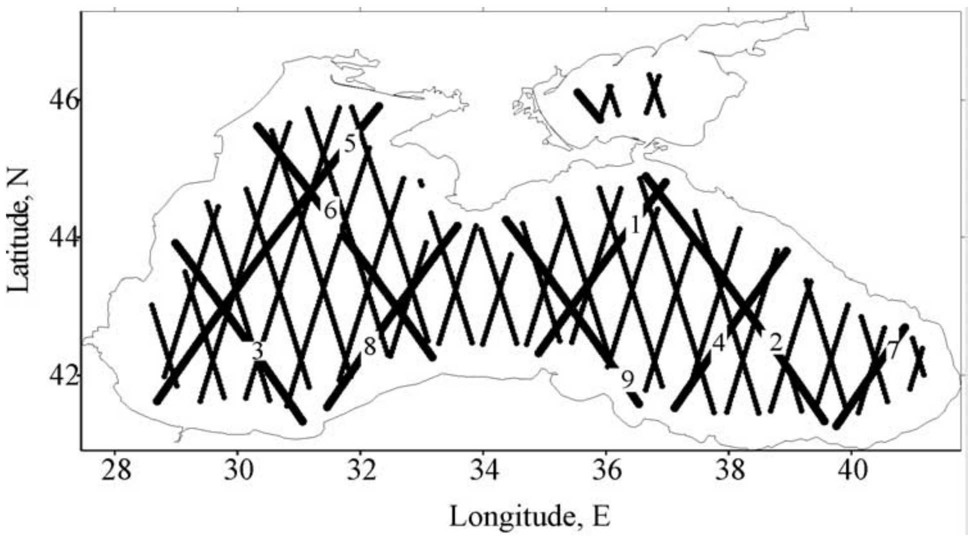

Figure 2. Tracks of TOPEX/Poseidon (thick lines) and ERS-I, II (thin lines) for the Black Sea [after *Korotaev et al.*, 2001].

signatures as well as some robust mesoscale features of the upper layer circulation system. A summary and discussion of results are given in section 6.

2. Altimeter Data Processing and Analysis

[5] The present study uses a combination of the data from both T/P and ERS-I, II altimeters covering the Black Sea along the tracks shown in Figure 2 with repeat cycle periods of approximately 10 and 35 days, respectively, for the 7 years spanning from May 1992 to May 1999. The data were preprocessed by the NASA Ocean Altimeter Pathfinder Project at Goddard Space Flight Center for atmospheric, sea surface and geoid corrections as well as filtering of erroneous data outside some prespecified limits [*Koblinsky et al.*, 1999]. The data set was further processed for the Black Sea conditions following *Korotaev et al.* [2001]. In particular, a 30 km coastal zone dominated by enhanced wave activity was excluded by the original data set, the data along each track were smoothed by a three-point running average, and then subtracted by the along track mean so that each track was given a zero mean. Additional corrections were applied to exclude the influence of seasonal sea level changes because of river runoffs, evaporation, precipitation, atmospheric load effect, and steric oscillation. The proposed correction is based on the assumption that the response of the basin to low-frequency variability of the volume flux is almost uniform in space. A simple theoretical analysis using the quasi-geostrophic dynamics (not provided here) suggests that this is a valid approximation for the Black Sea. Tidal correction was neglected, because of its negligible importance in the Black Sea.

[6] The contribution of the fresh water fluxes (evaporation, precipitation, river discharge and strait exchanges) to the sea level variations was estimated by averaging the sea level anomaly data along the tracks. The mean was then removed from the actual sea level anomaly values along these tracks in order to assign each track a zero mean. However, subtracting the mean values at each data point also removes the contribution of the ⟨time meant⟩ circulation. This loss was then compensated approximately by adding along the tracks the mean sea level obtained from the climatological hydrographic data [*Altman et al.*, 1987] using the method described by *Korotaev et al.* [2001]. Finally, the annual mean sea level simulated from the climatological hydrographic data (Figure 3) is added to obtain the absolute dynamical sea level. The resultant along-track sea level data, called hereinafter as the dynamical sea levels (DSL), were then optimally interpolated onto the model grid using decorrelation scales of 30 km and 23 days. Validation of the altimeter data processing has been given earlier by *Korotaev et al.* [2001] using four specific hydrographic survey data.

3. Assimilation of the DSL Data

[7] The conventional statistical interpolation approach using optimal mapping of the DSL fields described in the previous section as well as by *Korotaev et al.* [2001] is extended here to the case of dynamical interpolation approach through assimilating the DSL data in a model. The novel feature of the dynamical interpolation is to provide a dynamically consistent estimation of temporally

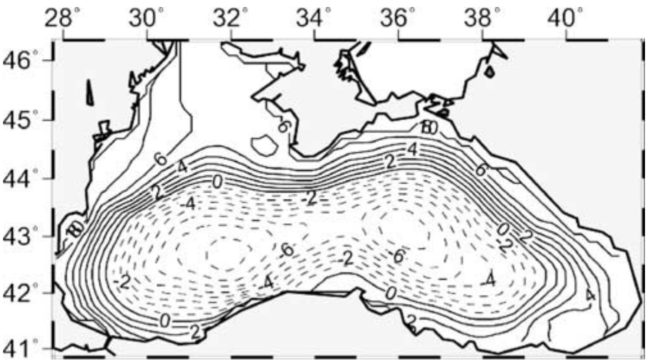

Figure 3. The annual mean sea level distribution (in cm) obtained from the climatological hydrographic data. The contours are plotted at an interval of 1 cm.

evolving fields, and extending the data information beyond the variable that is observed to properties not directly measured. In our case, the observed data being limited to sea level measurements is utilized to estimate current fields in the upper ~100 m layer of the water column separated from the deep homogeneous layer of ~2000 m by a steep pycnocline. The existence of two layer stratification and associated flow structure with weak subpycnocline currents in the Black Sea justifies the choice of relatively simple model based on the fully nonlinear, 1.5 layer reduced gravity, shallow water equations, except the northwestern shelf (NWS). A quasi-geostrophic version of the 1.5 layer reduced gravity model [*Korotaev et al.*, 2001], which has been found to be adequate to obtain the first-order dynamical response of the basin to the wind stress forcing, further supports our choice of the model. Even though the reduced gravity approximation is formally questionable for the NWS, the model-derived results were found to be consistent with those provided by optimal mapping as well as the features suggested by the hydrographic and satellite data for this particular region. This simple model does not allow spontaneous generation of mesoscale eddies by its internal dynamics and, as will be shown below, eddies are provided by the altimeter data assimilated into the model.

[8] The altimeter data is assimilated by employing the relaxation approach, whose flexibility and effectiveness have been reported by *Hurlburt* [1986], *Forbes and Brown* [1990], *Haines et al.* [1993], *Smedstad and Fox* [1994] as compared to more complex methods such as an approximate Kalman filter [*Fukimori*, 1995], adjoint approach [*Greiner and Perigaud*, 1994], variational assimilation method [*Weaver and Anderson*, 1997]. For an exhaustive review on application of assimilation techniques to altimeter data, we refer to *Fukumori* [2001].

[9] The equations governing the motion for the 1.5 layer reduced gravity model are expressed by

$$\frac{\partial(h\vec{v})}{\partial t} + \nabla\cdot(h\vec{v}\,\vec{v}) + f\times\vec{k}(h\vec{v}) = -g'h\nabla h + \frac{\vec{\tau}}{\rho_0} + A_h\nabla^2(h\vec{v}) \quad (1)$$

$$\frac{\partial h}{\partial t} + \nabla(h\vec{v}) = \gamma[\xi_d - \xi_m] \quad (2)$$

where $\vec{v}$ is the horizontal velocity with the eastward u and northward v components, h is the layer thickness, h_0 is its equilibrium value, $\vec{\tau}$ is the wind stress, $f = f_0 + \beta y$ is the Coriolis parameter with β plane approximation, A_h is the Laplacian horizontal mixing coefficient, $\rho_0 = 1017$ kg m^{-3} is the reference density, $\rho_1 = 1013.8$ kg m^{-3} is the mean density of the upper layer, $g' = g(\rho_0 - \rho_1)/\rho_0$ is the reduced gravity with g the acceleration due to gravity, γ is the inverse of the relaxation time, $\vec{k}$ is the unit vector directed upward, and ∂ is the partial derivative with respect to time, ∇ denotes the horizontal gradient operator for differentiation in the x (east) and y (north) directions. The right hand side of (2) describes relaxation of the model predicted interface anomaly, $\xi_m = h - h_0$, to the observed value provided by the altimeter data, ξ_d, which is related to the observed sea surface anomaly η by $\xi_d = (g/g')\eta$ [*Hurlburt*, 1986].

[10] The basin includes neither Mediterranean underflow at the Bosphorus opening nor the river inputs discharging into the northwestern shelf since they are not crucially important aspects of the problem under consideration. Free slip conditions are imposed along the lateral boundaries. Equations are solved on a staggered C grid using the explicit finite difference method. The layer thickness is located at the center of each grid box of dimension 7860 m and 6950 m in x and y directions, respectively. The u and v points are located on meridional and zonal faces, respectively. The leapfrog technique is used in time and centered differences in space. The time splitting instability of the leapfrog scheme is controlled by smoothing the fields at every time step with the Aselin filter. Horizontal diffusion terms are evaluated at the backward time level and all other terms at the central time level. A time step of 10 minutes is used for integration of equations. Horizontal viscosity is taken as 50 m^2 s^{-1}. Using a typical density difference, $(\rho_0 - \rho_1)$ of 3.2 kg m^{-3} , and unperturbed layer thickness of $h_0 = 150$ m, the Rossby radius of deformation is estimated at about 22 km. The grid therefore resolves the mesoscale processes reasonably well. The model has been forced by the ECMWF wind stress data for the years 1988 through 1999. The model is spun up in prognostic form from the beginning of 1988 to May 1992, after which the altimeter data are assimilated at each time step by interpolating linearly from their daily fields.

4. Simulations Without Data Assimilation: Characteristics of The Pure Wind-Driven Circulation

[11] The climatological mean sea level data shown in Figure 3 yields the most prominent features of the Black Sea upper layer circulation system known since *Knipovich* [1932]. These are the presence of a well-defined cyclonic circulation, characterized by a basin wide cell with two subbasin-scale gyres in each of the two basins. The mean sea level pattern also reveals an anticyclonically dominated narrow zone around the periphery, but without any particular anticyclonic eddy activity. The absence of mesoscale features should possibly be due to its coarse resolution, about 1°, of the *Altman et al.* [1987] climatological data.

[12] When the restoring term on the right hand side of (2) is omitted, our simple model is run in its prognostic mode forced by the wind stress alone. The sea surface anomaly fields, shown in Figures 4a and 4b at central days of

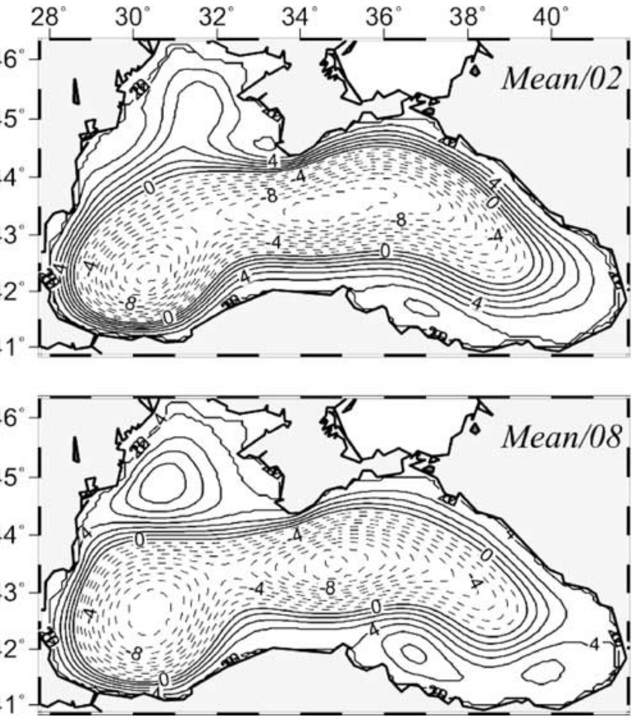

Figure 4. The 7 year mean DSL patterns simulated by the prognostic model for (top) mid-February and (bottom) mid-August. The ontours are plotted at an interval of 1 cm.

February and August as the 7-year averages over the simulation period, indicate that the wind forcing produces the most fundamental element of the Black Sea circulation. It is the year-round cyclonic cell throughout the basin and resembles that given by the climatological mean sea level pattern in Figure 3 with some minor seasonal changes. Two noticeable of these changes are the anticyclones on the southeastern and northwestern corners of the basin during the warm part of the year (Figure 4b). The simplicity of the model dynamics due to the absence of baroclinic and frontal instability processes as well as the absence of thermodynamics may be responsible for temporal uniformity in the circulation patterns. While the lack of instability processes in the model prevents spontaneous generation of eddies, the absence of thermodynamics ignores temporal and spatial variations of the density field and subsequently baroclinic contribution to the pressure gradient term in (2). As far as the sea level variations are concerned, we note that more sophisticated, eddy-resolving multilevel models introduce only a limited additional spatial complexity under wind-dominated circulation regimes [see, e.g., *Stanev and Staneva*, 2001, Figure 2; *Staneva et al.*, 2001, Figures 1a, 1c, and 1e].

5. Simulations With Data Assimilation

[13] set of sensitivity experiments has first been carried out to assess optimum values of the model parameters which provide an optimal fit of the dynamic model to the observations. We found that the simulated fields do not sensitive to variations of the layer depth and density difference between the layers in the range of their values given above. When the relaxation timescale is set to 10 days, the sea surface anomaly

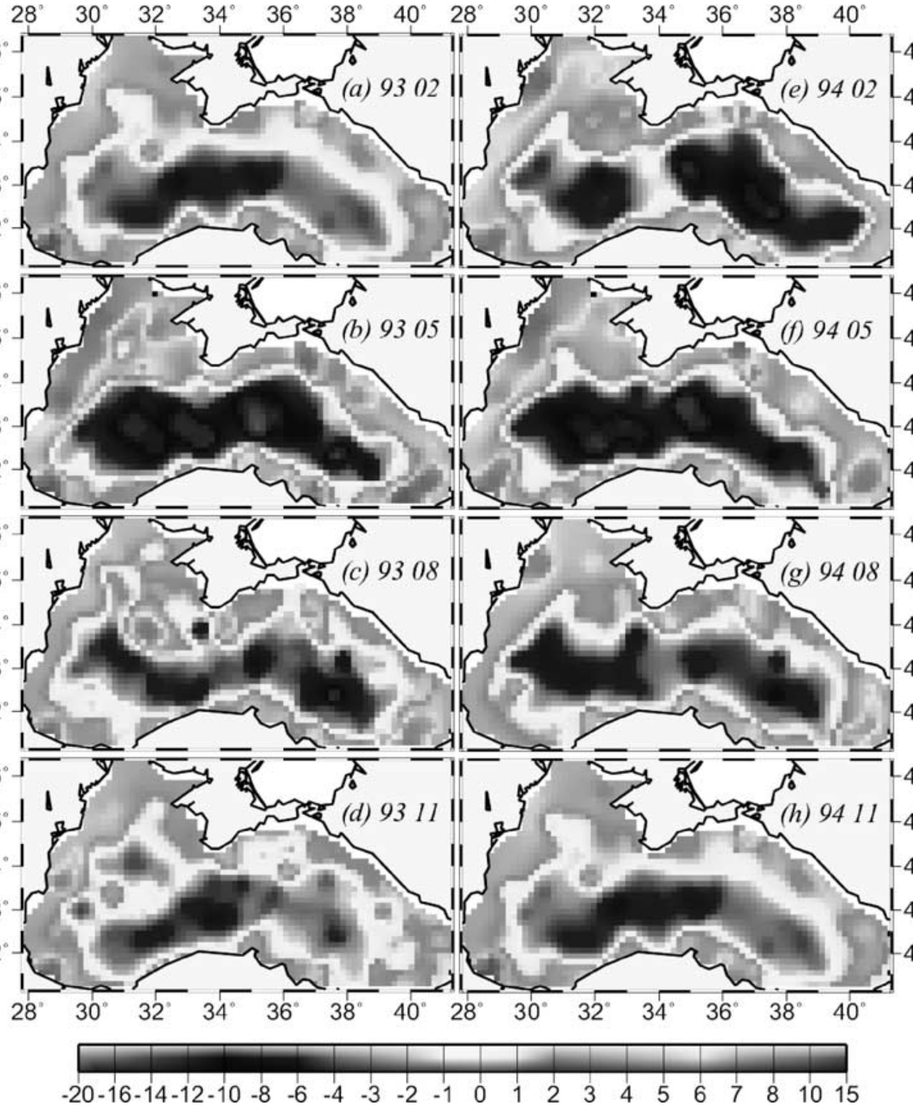

Figure 5. DSL anomaly maps (in cm) derived from assimilation of altimeter data into the model for the years (left) 1993 and (right) 1994 during (a) and (e) mid-February, (b) and (f) mid-May, (c) and (g) mid-August, and (d) and (h) mid-November. See color version of this figure at back of this issue.

fields differ only slightly from its prognostic counterparts, implying that the choice γ = 1/10 d^{-1} does not impose sufficiently strong control of the assimilation. On the other hand, lower values of the relaxation timescale progressively allow for faster convergence toward the observations. The values of the relaxation time less than three days were found to capture the altimeter signal quite realistically with only minor differences. Then, γ = 1/2 d^{-1} is accepted as the standard value of the relaxation parameter for the simulations described in the rest of the paper. This choice of the relaxation parameter, when combined with simplicity of the model physics, results in the DSL fields very similar to those obtained directly by optimal mapping procedure outlined in section 2. This has been verified by comparing the model results with the products shown by *Korotaev et al.* [2001]. Similar compatibility is also observed between the model-derived flow fields and those computed geostrophically by the optimally produced DSL maps. Thus the dynamical interpolation approach adopted in the present work simply serves an alternative to the statistical interpolation approach used in our earlier work [*Korotaev et al.*, 2001].

5.1. Seasonal and Interannual Variations of the Circulation System

[14] The dynamical sea level anomaly fields for all the years from May 1992 to May 1999 show a remarkably persistent signature of the seasonal flow structure, examples of which are shown in Figure 5 for the central days of February, May, August and November for the years 1993 and 1994. The winter circulation structure (Figures 5a and 5e) only slightly differs from that of the temporal mean circulation (Figure 3), and involves a two-gyre system decoupled from each other by a narrow zone roughly around 33°–34°E. The eastern gyre extends southeastward up to the eastern coast and is almost twice the size of its western counterpart. The connection of these gyres with each other along the northern and southern coasts leads to an uninterrupted basin wide peripheral circulation system.

Depending on the severity of winter meteorological conditions, year-to-year variability exists with higher DSL values corresponding to more intense cyclonic gyral circulation. For example, during the winters of 1993, 1996, 1997 and 1998, the gyres attain uniform structure characterized by DSL values of more than 10 cm (Figure 5a). On the other hand, during those of 1994, 1995 and 1999, only the central parts of the gyres are characterized by deepest DSL anomalies, implying a weaker and broader peripheral circulation (Figure 5e). The stronger cyclonic circulation is generally accompanied by equally strong anticyclonic type coastal recirculation zones around the periphery.

[15] The winter conditions typically persist for January, February and March, after which the circulation structure evolves to its subsequent spring phase during April, May and June. The most distinctive feature of the spring DSL fields, shown in Figures 5b and 5f by the May patterns, is the transformation of the two-gyre system into one composite basin wide cyclonic cell. While the DSL structure within the central parts of the interior cell remains as deep and strong as in winter, it reveals a milder slope around the periphery suggesting a weaker, but broader Rim Current zone. The Batumi eddy (see Figure 1 for its location) which was absent in winter months is formed near the southeastern corner of the sea during the spring period.

[16] In summer months (July, August, September), the interior circulation regime is subject to further weakening. The August DSL patterns (Figures 5c and 5g) suggests breaking of the interior cell into a series of smaller cyclonic eddies having typical dimensions of the order of 100 km. This structure is however subject to some interannual variability. For example, the weaker and smaller eddy-dominated systems during 1993, 1994, and 1997 differ from relatively more composite and stronger systems during 1995, and 1996. The Rim Current structure around the interior cell is therefore subject to a more pronounced mesoscale variations as compared to winter months. The Batumi eddy continues to persist during the summer months.

[17] The summer circulation of the interior basin continues to weaken and to disintegrate into smaller-scale cyclonic features during the autumn (October, November, and the first half of December). As can be noted by the November DSL maps (Figures 5d and 5h), the circulation system possesses its most disorganized structure, being completely opposite to the winter case. The Rim Current attains its weakest intensity of the year, and is subject to a great deal of lateral variability associated with the prevailing disorganized basin wide flow system. The most extreme cases for such events are observed during 1993, 1994 and 1998. The Batumi eddy weakens during this season. This type of turbulent, eddy-dominated flow system is then converted to a fully organized and more intense structure within the next couple of months starting by mid-December.

5.2. Mesoscale Features Along the Anatolian Coast

[18] The position of the Rim Current jet axis follows a year-round, almost persistent track along the southern and northern boundaries. The major axis of the Rim Current is closer to the coast in the south, and is generally characterized by smaller amplitude meanders. The interior waters may therefore penetrate up to the coast at certain sections of the coastline. The coastal side of some of these meanders are occupied by mesoscale anticyclonic eddies, the most persistent of which is the Bosphorus eddy present almost in all of the DSL patterns near the western corner of the south coast. The next persistent coastal feature with almost identical annual cycles every year is the Batumi eddy located at the other end of the south coast. Its time evolution is shown in Figures 6a–6f for the year 1993, and repeats with ±1–2 weeks difference in initiation and dissipation periods in other years. It begins to form in February as a small anticyclonic vortex with a size less than 100 km near the coast (Figure 6a). It then grows gradually in spring by expanding toward the interior of the eastern basin and elongating north along the Caucasian coast (Figure 6b). This feature persists throughout the spring, summer and early autumn (Figures 6c and 6d). It finally disintegrates into smaller eddies in October (Figure 6e) and dissipates all together in November as the circulation system begins to switch to its winter regime (Figure 6f).

[19] The Sakarya, Sinop and Kizilirmak eddies of the south coast (see Figure 1 for their locations) appear to be not as quasi-persistent structures as the Batumi and Bosphorus eddies. They may form recurrently once or twice a year for about a season. When they are sufficiently large, the Sinop and Kizilirmak eddies may be combined and form a single entity. The presence of these three eddies mostly depends up on propagation characteristics of the meanders superimposed on the Rim Current system. Thus these coastal eddies may be displaced occasionally from their positions indicated in Figure 1. The preferential direction of the wave propagation is counterclockwise, which is eastward along the south coast and westward along the northern coast as documented earlier by *Sur et al.* [1994], *Oguz and Besiktepe* [1999] and others.

[20] Figure 7 shows five particular snapshots of daily flow fields along the Anatolian coast during August–December 1997. Figure 7a, describing the conditions during 20 August 1997, reveals five coastal anticyclonic eddies and a series of meanders associated with them. The coastal zone to the west of $\sim 31°$E is covered by a composite elongated eddy, which may be regarded as an eastward extension of the original Bosphorus eddy. The region between 31° and 36°E includes the Sinop and Kizilirmak eddies as well as a third one located along the curved coastline between 31° and 32°E. The eastern part of the basin possesses almost no mesoscale activity except the Batumi eddy. The circulation maps for 20 September and 20 October 1997 (Figures 7b and 7c) suggest evolution of this flow field into a more complex system. In particular, the Bosphorus and Sakarya eddies emerge as two independent features, and the Sinop eddy splits into two parts. More active meandering structure of the Rim Current and two new coastal eddies appear in the region between the Kizilirmak and Batumi eddies. The small anticyclonic feature, which is referred to as the Sukhumi eddy here, is formed along the Caucasus coast to the north of the Batumi eddy. Within a month, the coastal eddy activity generally weakens, the Bosphorus and the Sakarya eddies are combined with the adjacent eddy to form one single entity covering the entire coastal zone up to 32°E (Figure 7d). At the same time, the Sinop and Kizilirmak eddies disappear and the Batumi eddy disintegrates into two smaller eddies. The meanders grow and expand offshore, and thus are characterized by larger amplitudes. Further

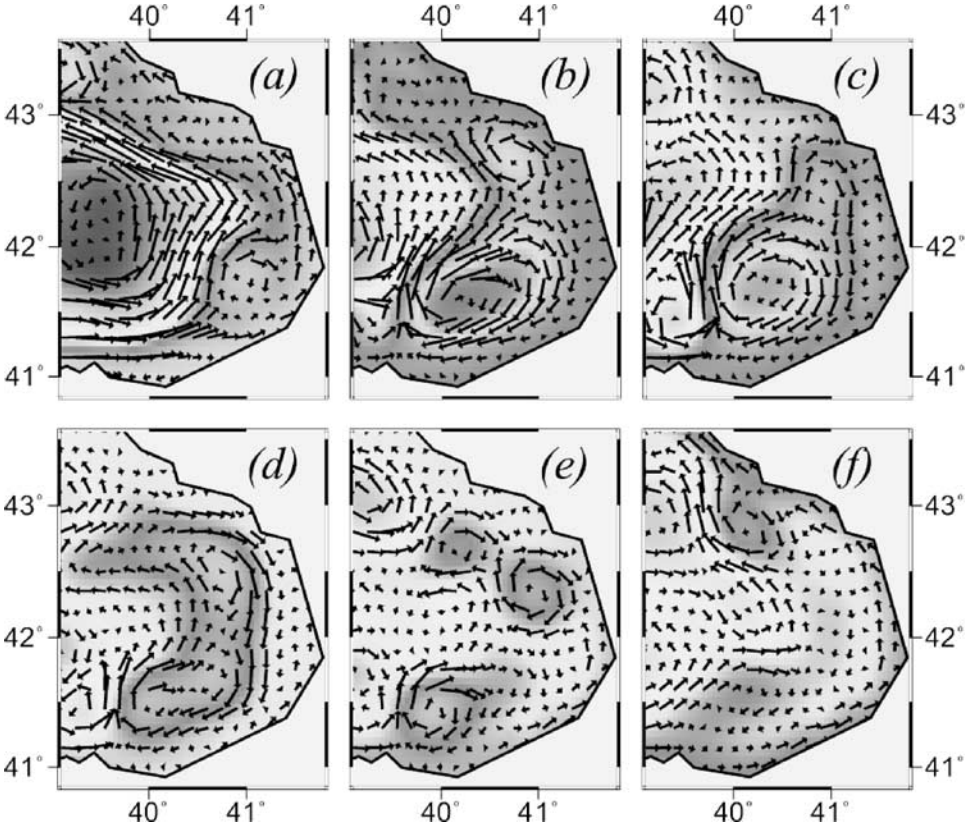

Figure 6. The evolution of the flow field in the Batumi gyre region showing its formation, development and disintegration during (a) 31 January 1993, (b) 30 April 1993, (c) 30 July 1993, (d) 10 October 1993, (e) 30 October 1993, and (f) 30 November 1993.

evolution of the system takes place in December (Figure 7e). The eddy centered at 39°E protrudes offshore in the form of a mushroom structure, and the Sukhumi eddy merges with the remnant of the Batumi anticyclone.

5.3. Mesoscale Features Along the Caucasian Coast

[21] Along the Caucasian coast, from the Batumi eddy region at its southeastern end to the vicinity of the Kerch Strait at the northwestern end, the axis of the Rim Current jet is located further away from the coast, giving rise to larger amplitude meanders and a broader zone of anticyclonic eddies. The so-called Caucasian eddy is a quite persistent structure of this region and is often associated with a large offshore protrusion of the Rim Current jet toward the interior of the eastern cyclonic gyre. The region to the south of the Kerch Strait exhibits another persistent anticyclonic eddy. It is seen in almost all the DSL maps and will be referred to as the Kerch eddy here.

[22] The altimeter data suggest that the Kerch and Caucasian eddies are not completely decoupled features, but interact with each other and the Rim Current, and therefore constitute elements of a temporally evolving local flow system along the Caucasian coast. Figures 8a–8d show a sequence of events for this system during spring-summer 1993. The regional flow field is characterized by the Sukhumi, Caucasian and Kerch eddies along the coast and a broad band of the Rim Current at their offshore side during 30 April 1993 (Figure 8a). The Caucasian and Kerch eddies are separated from each other by a sharp onshore meander of the Rim Current. Within a month, the Caucasian eddy grows and elongates on both sides along the coast, and absorbs the Sukhumi eddy during the end of next month (Figure 8b). Its northwestward movement along the coast first weakens the meander of the Rim Current, and then leads to its merging with the Kerch eddy in June 1993 (Figure 8c). The Caucasian coast then reveals a broad anticyclonic eddy persisting for a month. It then gradually deforms into a smaller-scale eddy and is finally lost while the Kerch eddy persists at its original location. The small anticyclonic eddy between the northwesterly currents on both onshore and offshore flanks soon takes the form of a well-defined new generation Caucasian eddy (Figure 8d).

[23] The Caucasian eddy and the associated Rim Current meander system at its outer flank are frequently seen to protrude offshore in the form of a filament. Figures 9a–9f display an evolutionary process for such an event during December 1996 to April 1997 period. The Caucasian eddy, embedded within a typical low meander state of the local flow field during 10 December 1996 (Figure 9a), gradually expands both toward the interior of the eastern basin and northwestward during December and January (Figures 9b and 9c). This process is accompanied by spontaneous generation of a new short-lived eddy along the offshore flank of the meander (Figure 9c), which is later detached and is finally absorbed by the interior basin circulation in February (Figure 9d). The meander and eddy system are then displaced toward the Kerch eddy. Following the next secondary eddy generation and subsequent detachment processes in February and

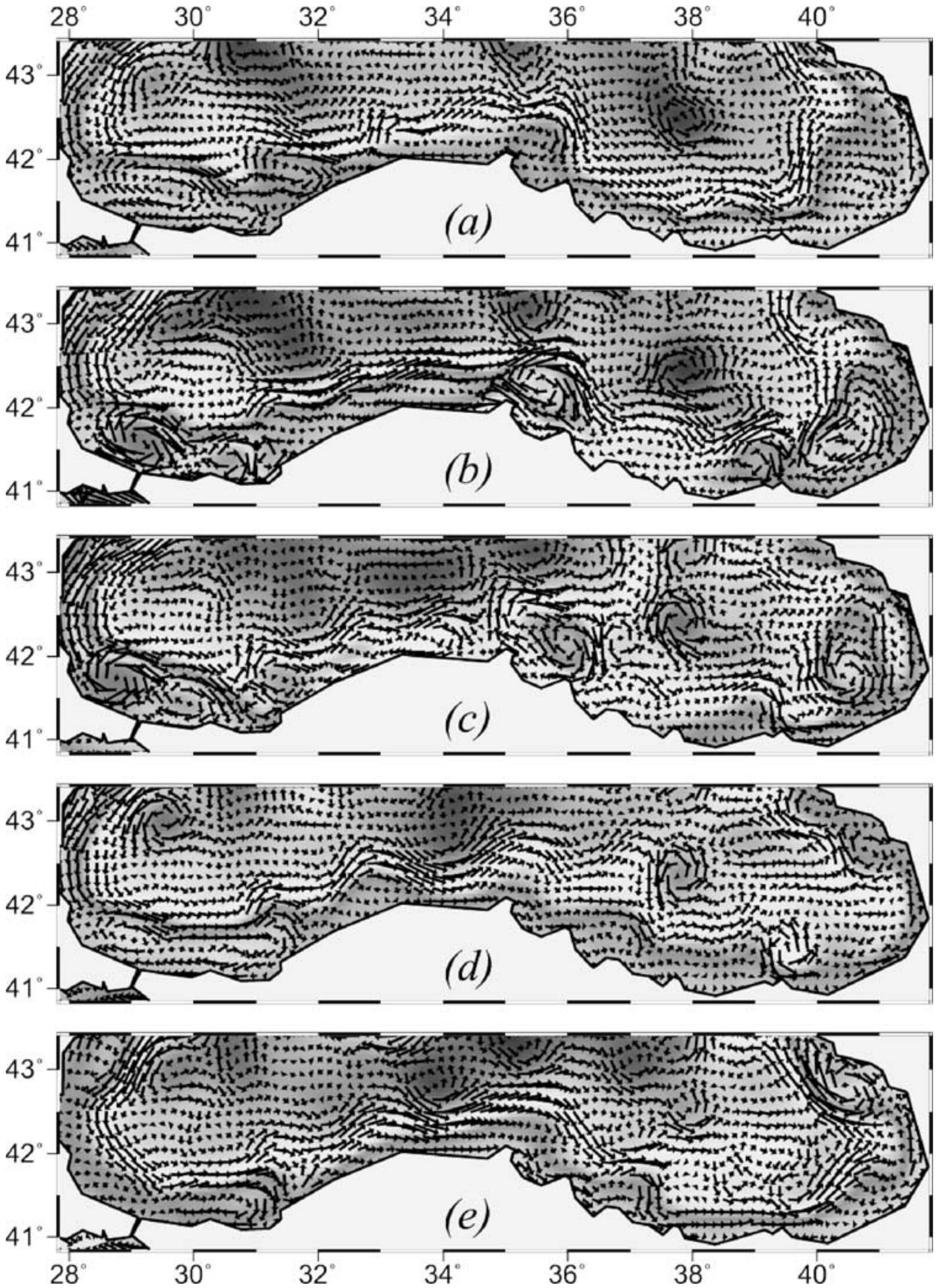

Figure 7. Evolution of the flow field along the Anatolian coast during (a) 20 August 1997, (b) 20 September 1997, (c) 20 October 1997, (d) 30 November 1997, and (e) 30 December 1997.

March 1997 (Figures 9d and 9e), the system eventually reverts back in April 1997 to its low meander state characterized by several small-scale coastal eddies (Figure 9f).

[24] Another example for the offshore protrusion of the Caucaus meander and its interaction with the features of the south coast is shown in Figures 10a–10d. During 11 January 1998, the Rim Current system along the Anatolian coast exhibits an offshore filament extending eastward along 42°N into the central part of the eastern basin (Figure 10a). Within a week, this feature is combined with an isolated anticyclonic eddy located within the interior to form a new filament which almost extends up to the Caucasian coast (Figure 10b). During the subsequent 10 day period, this filament is detached from its base at the south coast. The detached eddy then merges with the meander of the Caucasus coast leading to formation of a new offshore filament extending toward the interior from the northern coast (Figure 10c). Following its persistence for about two months, it is finally transformed into a pinched-off anticyclonic eddy occupying the central part of the eastern basin during the late-March and April 1998 (Figure 10d).

5.4. Mesoscale Features Along the Crimean Coast

[25] Two quasi-persistent coastal anticyclones are located on both sides of the Crimean peninsula. The one located on the eastern side, called the Crimean eddy, is generally

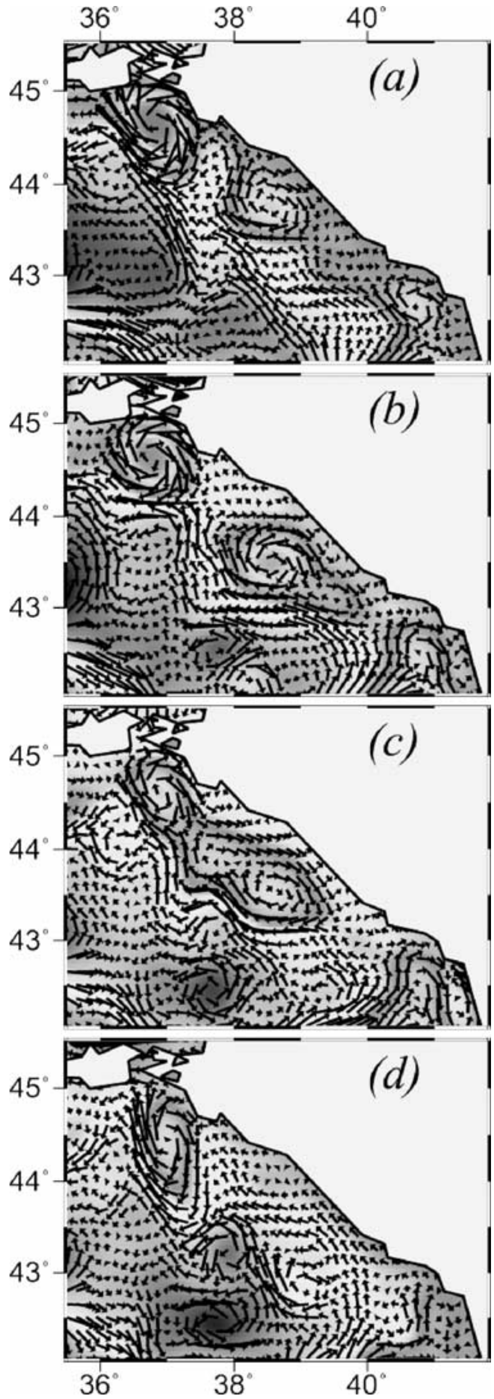

Figure 8. Evolution of the flow field along the Caucasus coast during (a) 30 April 1993, (b) 30 May 1993, (c) 20 June 1993, and (d) 10 August 1993.

attached to the tip of the headland. The other one located on the western side of the peninsula is known as the Sevastopol eddy. Its location depends on the local structure of the Rim Current which, constrained by local topographic control, flows mainly southwest along the topographic slope zone between the northwestern shelf and the western interior (see Figure 1 for the topography). Closer inspection of the instantaneous circulation maps in fact identifies two forms of the Rim Current path leading to formation of the Sevastopol eddy. One of them involves intense offshore meandering near the southwestern side of the tip of the Crimea. The eddy is then formed inside the meander. The other is the northward bifurcation of the Rim Current on the western side of the Crimean peninsula. In this case, the eddy is confined between the northward current system and the coast. Specific examples for each of these formation events are shown in Figures 11–13.

[26] Figure 11a shows the regional flow structure during 1 January 1993 prior to the Sevastopol eddy formation. The local circulation system is characterized by a well-defined Rim Current jet flowing along the topographic slope zone, a large anticyclonic eddy between the Romanian and Crimean coasts of the northern shelf, and a small and weak cyclonic eddy along the western coast of the Crimea. On the southwestern side of the Crimean peninsula, the Rim Current first deflects south toward the center of the western basin, and then swings clockwise north into the shelf. It then turns west-southwest and flows along the shelf break. Ten days later, an anticyclonic eddy is formed near the tip of the headland as a byproduct of the meander intensification (Figure 11b). As the meandering path of the Rim Current deforms later in January, the eddy grows in size, and translates slightly westward. At the same time, it interacts with the anticyclonic eddy of the shelf (Figure 11c) and finally form one composite north-south elongated structure toward the end of February 1993 (Figure 11d). A new Sevastopol eddy formation event initiates simultaneously near the tip of the Crimea.

[27] The Rim Current does not always possess a sharp offshore meander near the tip of the headland. Instead, as given by the regional flow pattern for 20 July 1995 in Figure 12a, it occasionally splits into two branches; one of them meanders westward by first swinging offshore and then onshore, the other turns northward and flows along the Crimean coast into the shelf. The northward branch contributes to the eddy formation within a week (Figure 12b), which then persists there for the next two months (Figure 12c) and finally weakens and is dissipated in October 1995 (Figure 12d). A more extreme example of this type of eddy formation mechanism is observed during summer 1996. The northward branch of the Rim Current undergoes a sharp meander, and accompanies two anticyclonic eddies on its shallower side and a cyclonic eddy in between on the offshore side (Figure 13a). The system intensifies during the next two months (Figures 13b and 13c), and is finally broken apart into a series of isolated mesoscale eddies in August 1996 (Figure 13d).

5.5. Mesoscale Features Within the NWS

[28] The flow system within the northwestern shelf (NWS) is governed by both intrusion of the Rim Current and discharges from the Danube, Dniepr and Dniestr Rivers; the discharge from the former is almost four times stronger than the sum of other two. The typical regional flow regime within the inner shelf is a southward coastal current system, which is denoted in the DSL maps (Figures 5a–5d) by yellow-to-red strips along the western coast. The outer shelf, on the other hand, is characterized by highly dynamic and complicated interactions between the inner shelf and the Rim Current flow systems as shown in Figures 11–13. The coastal fresh water-induced flow system includes some

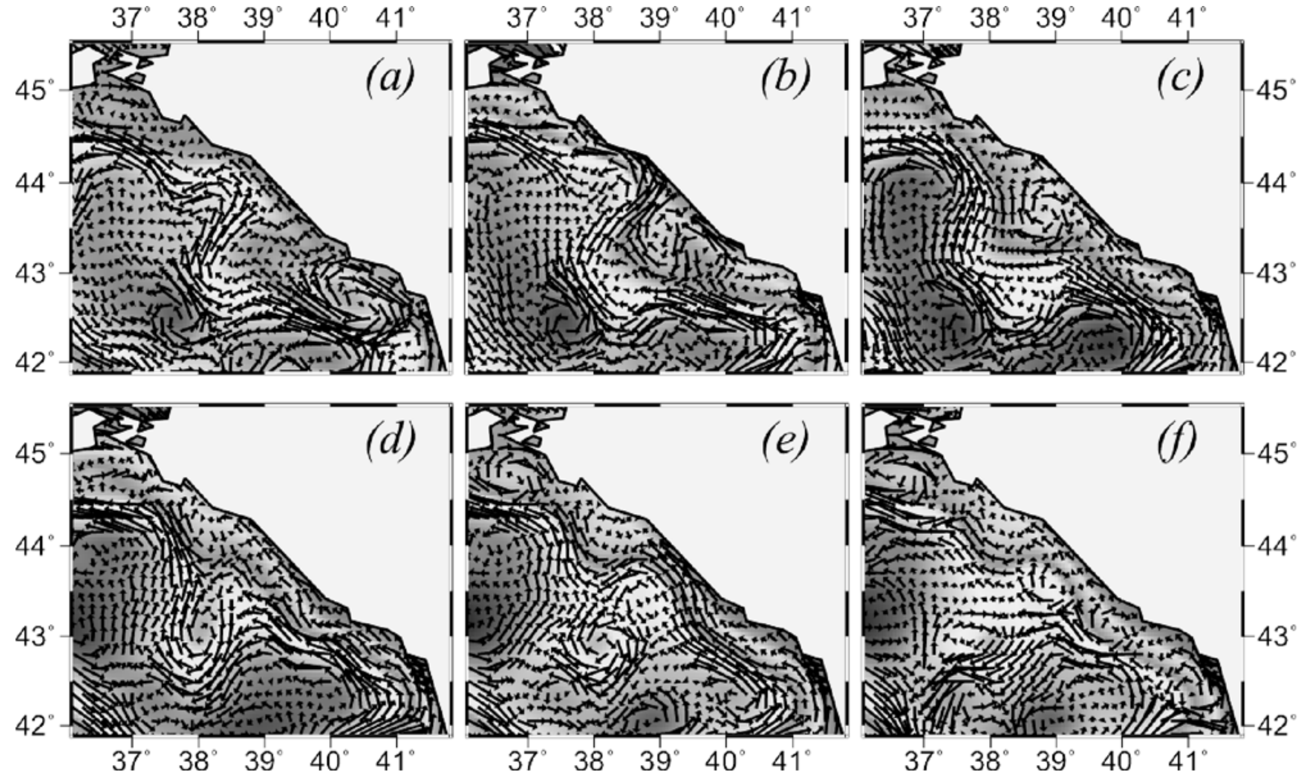

Figure 9. Evolution of the flow field showing a filament formation and subsequent eddy detachment events along the Caucasus coast during (a) 10 December 1996, (b) 30 December 1996, (c) 21 January 1997, (d) 20 February 1997, (e) 20 March 1997, and (f) 10 April 1997.

mesoscale anticyclonic eddies, one of which is located just outside the discharge zone of the Danube. The signature of this eddy is most evident in autumn DSL maps which reflect a weaker coastal current system due to considerable reduction in discharges. We refer to this feature as the Danube anticyclonic eddy. The other eddy is located slightly south near Cape Kaliakra, in the narrowest part of the northwestern shelf (see Figure 1). The Kaliakra anticyclonic eddy also emerges during the late summer and autumn months (see August and November DSL maps in Figures 5c–5d), whereas it is embedded within the coastal current system during high-discharge periods. Another small anticyclonic eddy is often present between the Danube and Kaliakra anticyclones. It will be called the Constantsa eddy here.

[29] Figures 11–13 provide some examples for various types of interactions between the shelf circulation and the Rim Current. The winter 1993 Sevastopol eddy formation event is accompanied by the Rim Current protrusion in the shelf, and then its flow along the shelf break toward southwest parallel to the coast (Figure 11). On its shallower side, the Danube and Kaliakra anticyclones are present. The Danube eddy occupies the entire northern part of the shelf (Figures 11a and 11b). Later, it splits into two parts by the northward intrusion of the Rim Current (Figure 11c). While the eastern eddy is eventually combined with the Sevastopol eddy (Figure 11d), the other one persists near the coast for some time. The Kaliakra eddy weakens during the same period and is combined with the Constantsa eddy.

[30] Somewhat different evolution of the shelf circulation and eddies takes place in summer 1995 (Figures 12a–12d). The Rim Current flows westward into the NWS along three different paths during 20 July 1995 (Figure 12a), which all turn south eventually and flow parallel to the coast. Once again, the inner shelf zone between the coast and the Rim Current is covered by three adjacent eddies as in the previous case. As these three eddies intensify during August (Figure 12c), the Danube eddy occupies the entire northern part of the NWS in September 1995 (Figure 12d) as in the case shown in Figures 11a and 11b. The coastal eddy structures of the NWS during the summer 1996 (Figures 13a–13d) are also similar. Once again the Rim Current penetrates into the shelf in three branches, the coastal zone is covered by the three adjacent eddies and the southward current system along the shelf break.

6. Summary and Discussion

[31] The present study makes use of the 7-year-long sea surface height anomaly data from the TOPEX/Poseidon and ERS altimeters since mid-1992 to describe the seasonal, interannual and mesoscale features of the upper layer circulation in the Black Sea. The altimeter data are interpreted by way of assimilation into a wind-driven, 1.5 layer shallow water model. This approach allows its dynamically consistent interpretation, and thus provides a more definitive and quantitative analysis for studying temporal and spatial characteristics of the circulation. Considering the fact that the available data provided by the hydrographic surveys and the SeaWiFS, AVHRR satellite sensors suffer from the lack of either proper spatial or temporal resolutions or both, their interpretations could never be generalized with confidence. From this point of view, the present study is a first

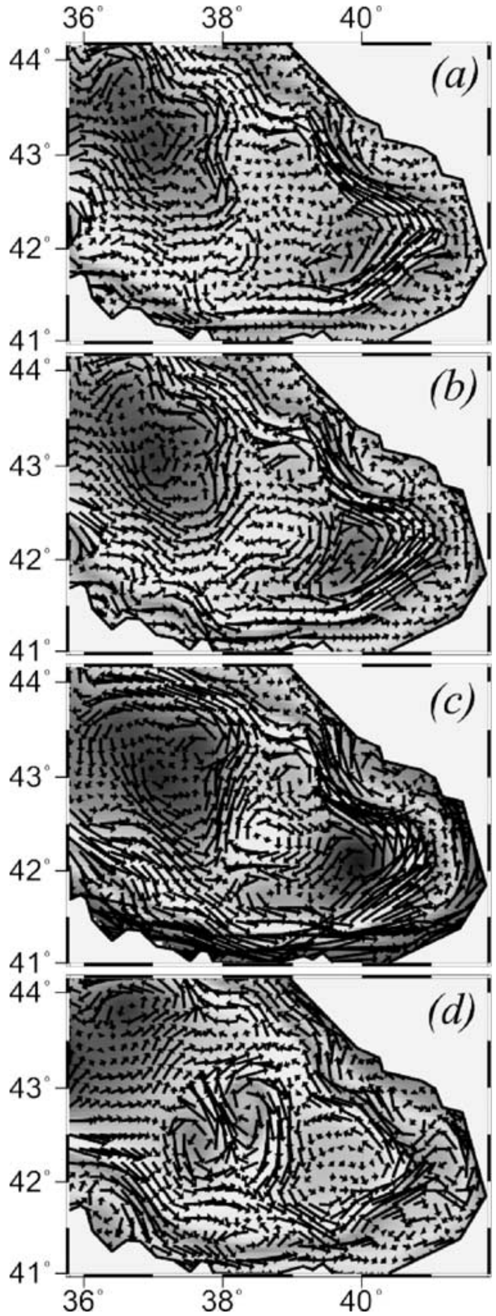

Figure 10. Evolution of the flow field showing interaction between the Caucasus and Anatolian coasts of the eastern basin (a) during 11 January 1998, (b) 21 January 1998, (c) 31 January 1998, and (d) 30 March 1998.

attempt to obtain a more reliable interpretation of the Black Sea circulation characteristics using a relatively long (i.e., 7 years) and spatially resolved data set. Verification and validation of the altimeter data products against a set of quasi-synoptic hydrographic surveys have already been described by *Korotaev et al.* [2001] and *Sokolova et al.* [2001].

[32] The rate of change of the basin-integrated total energy and the basin-integrated wind stress work computed using the altimeter data exhibit remarkably similar temporal variations throughout the observation period. This implies that the wind stress forcing exerts the major control on the upper layer circulation system, which is further modified by internal dynamical and thermodynamical processes. The purely wind-driven prognostic model simulations, in addition to simulating the basin-scale cyclonic cell, reveal two anticyclonic gyres near the southeastern and northwestern corners during the summer and autumn months. The presence of quasi-persistent Batumi and Danube eddies in the

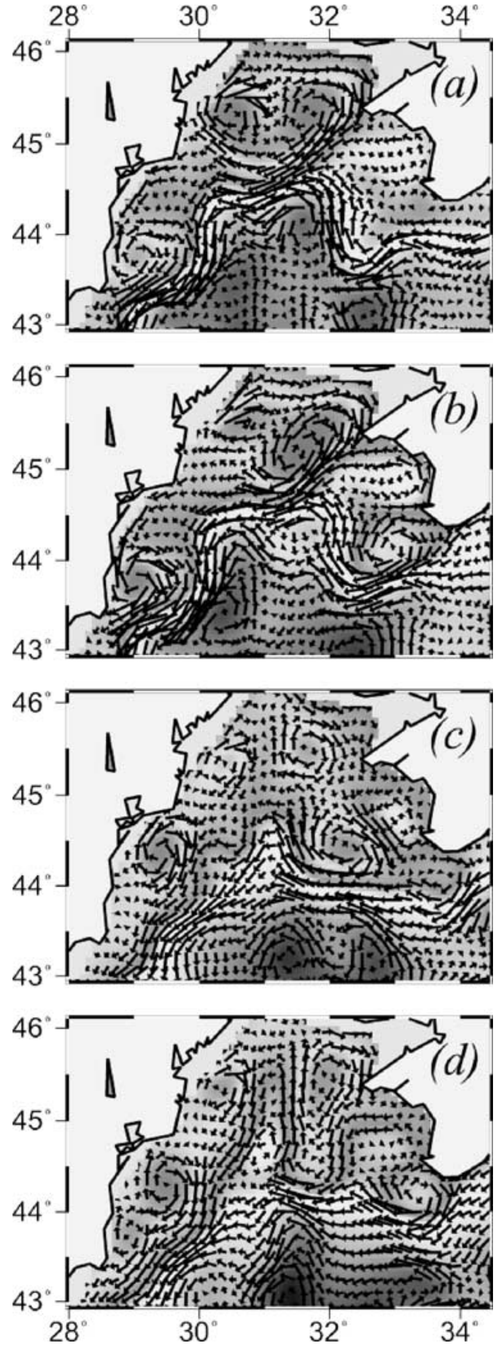

Figure 11. Evolution of the Sevastopol, Danube, Constantsa, and Kaliakra eddies in the northwestern region during (a) 1 January 1993, (b) 11 January 1993, (c) 10 February 1993, and (d) 28 February 1993.

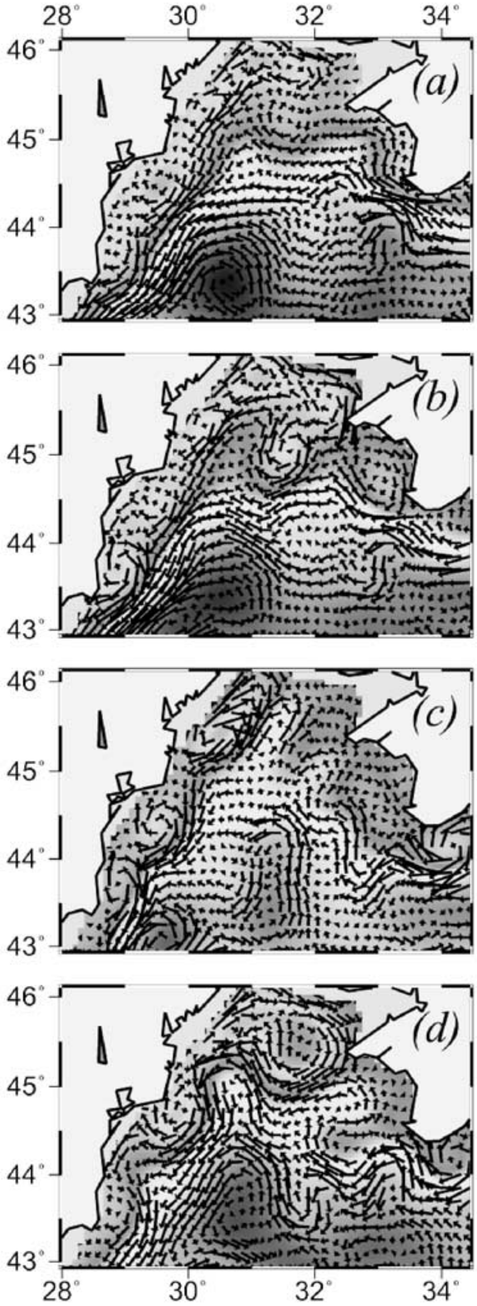

Figure 12. Evolution of the Sevastopol, Danube, Constantsa, and Kaliakra eddies in the northwestern region during (a) 20 July 1995, (b) 30 July 1995, (c) 30 August 1995, and (d) 30 September 1995.

altimeter data within these areas suggests that their energy is primarily provided by the wind forcing; the fresh water plume dynamics further modify the regional flow field in the northwestern shelf. This may explain the upstream deflection of the fresh water induced coastal current system frequently encountered in satellite and hydrographic data. The dynamics of river plumes, frontal instabilities and their interactions with the slope current of the basin wide circulation system further modify this background regional circulation pattern.

[33] Altimeter data reveal distinct seasonal cycle of large-scale characteristics of the circulation system repeating itself every year. Each winter season is identified by a two gyre system surrounded by a rather strong and narrow peripheral jet without any appreciable lateral variations. *Korotaev* [2001] has related the strengthening of the winter wind-

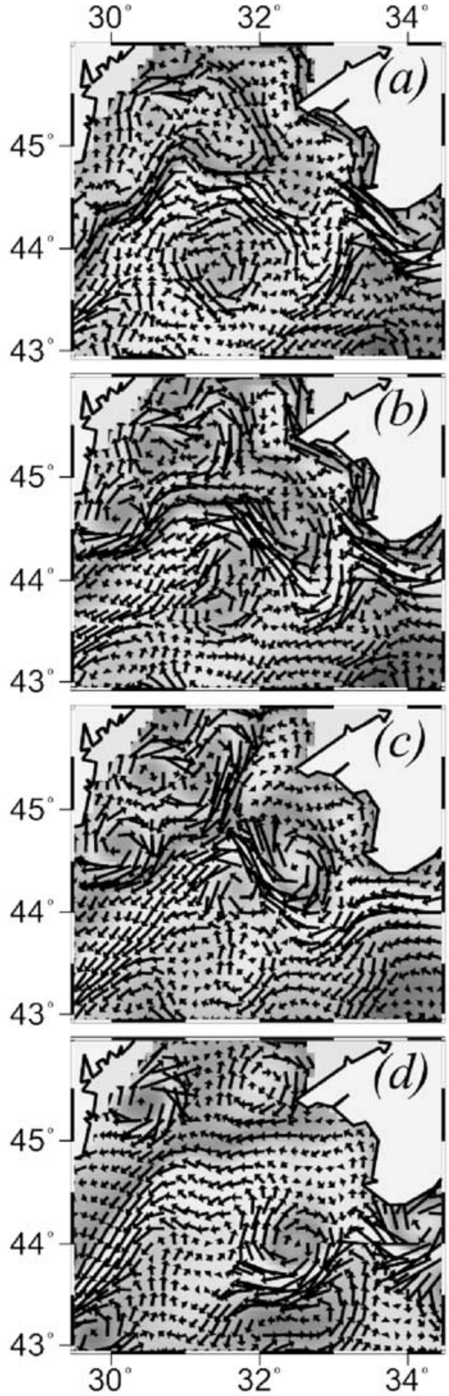

Figure 13. Evolution of the Sevastopol, Danube, Constantsa, and Kaliakra eddies in the northwestern region during (a) 20 June 1996, (b) 20 July 1996, (c) 30 July 1996, and (d) 20 August 1996.

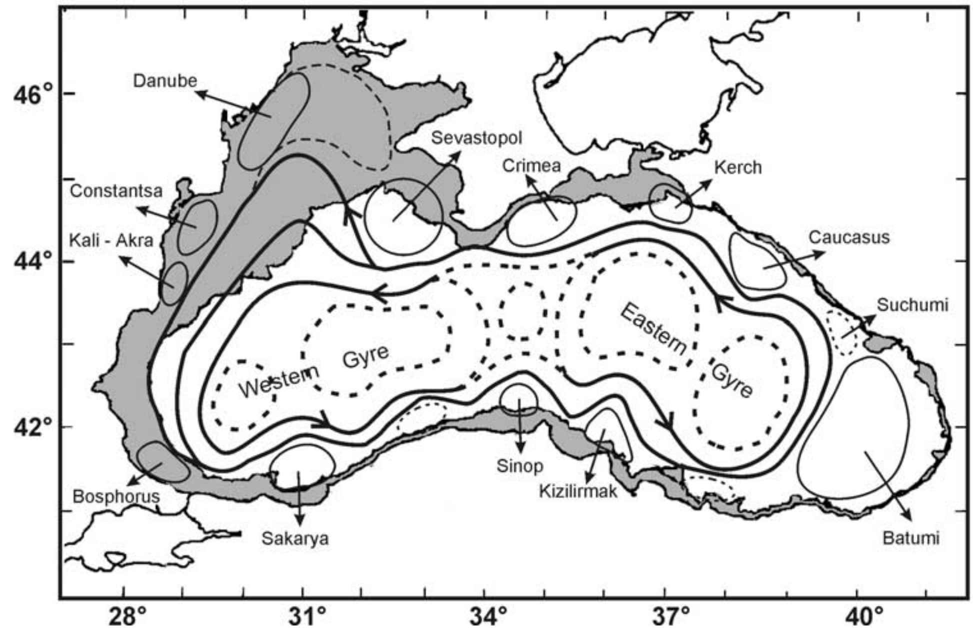

Figure 14. The revised schematic pattern including features derived from the analysis of the altimeter data.

driven circulation to the intense atmospheric system persisting over the Black Sea due to heating of the atmosphere by sea. The analysis suggested that higher heat loss from the sea during winters results in a stronger atmospheric cyclone and subsequently more intense circulation in the sea. The two-gyre system of winter months eventually transforms into one composite cyclonic cell surrounded by a broader and weaker Rim Current zone in summer. The interior basin flow field weakens further and finally disintegrates into smaller-scale cyclonic features in autumn. A composite peripheral current system is hardly noticeable in this season. The turbulent flow field is, however, rapidly converted into a more intense and fully organized structure after every November–December.

[34] The overall circulation system possesses a set of quasi-persistent and/or recurrent coastally attached anticyclonic eddies around the basin. Their persistence varies regionally and seasonally depending on the large-scale forcing of the circulation as well as on internal processes controlling the mesoscale dynamics. The most notable features include (i) the weakly meandering Rim Current system cyclonically encircling the basin, (ii) two cyclonic cells formed by four gyres distributed within the interior, (iii) the Bosphorus, Batumi, Sukhumi, Caucasus, Kerch, Crimea, Sevastopol, Danube, Constantsa, and Kaliakra anticyclonic eddies on the coastal side of the Rim Current zone, (iv) bifurcation of the Rim Current near the southern tip of the Crimea; one branch flowing southwestward along the topographic slope zone and the other branch flowing into the inner shelf and forming or contributing the southerly inner shelf current system, (v) convergence of the two branches of the original Rim Current once again along the Bulgarian and Turkish coast, (vi) presence of a large anticyclonic gyre within the northern part of the northwestern shelf.

[35] The analyses suggest that the energy of mesoscale features is primarily confined along the Rim Current jet. The typical timescale of the Rim Current meanders is found to be between 50 and 150 days. Evidence for the less intense, but quasi-periodic mesoscale variability introduced by Rossby wave propagation has been presented earlier by *Stanev et al.* [2000] and *Korotaev et al.* [2001]. The Bosphorus eddy is observed on the average for 260 days per year with a mean life time of about 85 days. Once it persisted for almost a year from mid-April 1993 until mid-March 1994. A chain of eddies along the Anatolian coast have more intermittent character and travel slowly eastward along the coast. The Sakarya, Sinop and Kizilirmak eddies tend to exhibit more quasi-permanent character due to controls exerted by regional topographies. The Batumi anticyclone is also among the most intense and persistent of the Black Sea coastal eddies. It regularly forms in early March and lives until the end of October; an average of 210 days per year. The Sukhumi eddy is manifested about 120 days per year and exists typically for about a month once it forms. It is mostly observed in autumn to early winter months when there is no Batumi gyre. The lowest probability of its observation corresponds to summer when it is absorbed by the Batumi gyre. It is formed either by detachment from the Batumi anticyclone at the end of its life cycle or by instability of the coastal jet radiated by the Batumi eddy or its predecessors. The Caucasus eddy appears about 160 days per year preferentially in spring months. Its average lifetime is about two months, but it may persist for up to nine months. It often interacts with the Sukhumi and Kerch eddies and is accompanied with a large offshore meander of the Rim Current into the central part of the eastern basin. The Kerch eddy is also one of the most pronounced features of the Black Sea eddy dynamics with an average persistence

of 240 days and a mean lifetime of 80 days. The spring and autumn seasons are found to be more favored periods for its presence. The Crimea anticyclone occurs mainly in August–September, and is observed around 115 days per year. The mean period for each event is about a month. The winter and summer are found to be most preferred periods for formation of the Sevastopol eddy. It is observed for about 150 days per year and has the mean life time of 50 days. It is generated as a byproduct of an intense meander of the Rim Current or as a part of bifurcation of the Rim Current along the western coast of Crimea. Detachment from the eastern periphery of the broad NWS anticyclone may also contribute to the formation process. The NWS is governed permanently by anticyclonic vorticity dynamics introduced by the wind forcing. For about 55% of the observation period, the anticyclonic vorticity is confined within a narrow band along the coast between Odessa and Constantsa. This is referred to as the Danube eddy, and it sometimes expands and occupies almost the whole NWS region. The Constantsa and Kaliakra anticyclones further south are observed for about 190 days per year with a typical lifetime of about 50 days.

[36] Most of the features of the Black Sea circulation system inferred from the altimeter data have already been pointed out a decade ago (see Figure 1) using the historical hydrographic and AVHRR data. These 7-year-long altimeter data provide an independent validation of the schematic picture presented in Figure 1, and introduce a few additional features. The revised schematic picture including all major quasi-persistent and recurrent features of the circulation pointed out in this study is given by Figure 14.

[37] In addition to identification of the seasonal and longer timescale features of the circulation, the altimeter data also provide numerous examples for highly dynamic events such as meander steepening and propagation, ring formation and detachment taking place at weekly timescales. The Caucasian and eastern part of the Anatolian coast as well as the topographic slope zone between the western interior and the northwestern shelf are the particular regions rich in mesoscale activities. As shown by the SeaWiFS chlorophyll data [*Oguz et al.*, 2002], such features can lead to considerable exchanges and transports between the coastal and offshore waters, and therefore constitute a crucially important component of the Black Sea dynamics and biogeochemistry.

[38] **Acknowledgments.** This work was made possible by the NATO Collaborative Linkage grant EST.CLG 975821 between T. Oguz and G. Korotaev, and the CRDF grant UG2-2081 between C. Koblinsky and G. Korotaev. T. Oguz also acknowledges partial supports by NSF Grant OCE9906656, and the Turkish Scientific and Technical Research Council (TUBITAK) project 101Y005.

References

Altman, E. N., N. F. Gertman, and Z. A. Golubeva, *Climatological Fields of Salinity and Temperature of the Black Sea Water* (in Russian), 109 pp., State Oceanogr. Inst., Sevastopol, Ukraine, 1987.

Besiktepe, S. T., C. J. Lozano, and A. R. Robinson, On the summer mesoscale variability of the Black Sea, *J. Mar. Res.*, *59*, 475–515, 2001.

Blatov, A. S., N. P. Bulgakov, V. A. Ivanov, A. N. Kosarev, and V. Tujilkin, *Variability of the Hydrophysical Fields in the Black Sea* (in Russian), 240 pp., Gidrometeoizdat, St. Petersburg, Russia, 1984.

Ducet, N., P. Y. Le Traon, and P. Gauzelin, Response of the Black Sea level to atmospheric pressure and wind forcing, *J. Mar. Syst.*, *22*, 311–327, 1999.

Forbes, C., and O. Brown, Assimilation of sea surface height data into an isopycnic model, *J. Phys. Oceanogr.*, *26*, 1189–1213, 1990.

Fukimori, I., Assimilation of TOPEX sea level measurements with a reduced-gravity shallow water model of the tropic Pacific Ocean, *J. Geophys. Res.*, *100*, 25,027–25,039, 1995.

Fukumori, I., Data assimilation by models, in *Satellite Altimetry and Earth Sciences*, pp. 237–265, Academic, San Diego, Calif., 2001.

Gawarkiewicz, G., G. K. Korotaev, S. Stanichny, L. Repetin, and D. Soloviev, Synoptic upwelling and cross-shelf transport processes along Crimean coast of the Black Sea, *Cont. Shelf Res.*, *19*, 977–1005, 1999.

Ginsburg, A. I., A. G. Kostianoy, D. M. Soloview, and S. V. Stanichny, Remotely sensed coastal/deep-basin water exchange processes in the Black Sea surface layer, in *Satellites, Oceanography and Society*, edited by D. Halpern, *Elsevier Oceanogr. Ser.*, *63*, 273-285, 2000.

Greiner, G., and C. Perigaud, Assimilation of Geosat altimetric data in a nonlinear reduced-gravity model of the Indian Ocean. part I: Adjoint approach and model-data consistency, *J. Phys. Oceanogr.*, *24*, 1783–1804, 1994.

Grishin, G. A., Satellite and ship-borne observations of hydrological fronts in the Black Sea and in the Mediterraneran Sea, *Sov. J. Remote Sens.*, *11*, 846–862, 1994.

Haines, K., P. Malanotte-Rizzoli, R. E. Young, and W. R. Holland, A comparison of two methods for the assimilation of altimeter data into a shallow-water model, *Dyn. Atmos. Oceans*, *17*, 89–133, 1993.

Hurlburt, H. E., Dynamic transfer of simulated altimeter data into subsurface information by a numerical model, *J. Geophys. Res.*, *91*, 2372–2400, 1986.

Knipovich, N. M., *The Hydrological Investigations in the Black Sea: Trans. Azov-Black Sea Expedition* (in Russian), vol. 10, 274 pp., Russ. Acad. of Sci., Moscow, 1932.

Koblinsky, C. J., R. Ray, B. D. Beckley, A. Brenner, L. Tsaoussi, and Y. M. Wang, Data set validation, *NASA Rep., 2*, 56 pp., 1999.

Korotaev, G. K., A reason of seasonal changes of the Black Sea circulation(in Russian), *Mar. Hydrophys. J.*, *6*, 14–20, 2001.

Korotaev, G. K., O. A. Saenko, C. J. Koblinsky, and V. V. Knysh, Satellite altimetry observations of the Black Sea, in *Environmental Degradation of the Black Sea: Challenges and Remedies*, *NATO Sci. Ser.*, vol. 2, *Environ. Security*, vol. 56, edited by S. Besiktepe et al., pp. 225–244, Kluwer Acad., Norwell, Mass., 1999.

Korotaev, G. K., O. A. Saenko, and C. J. Koblinsky, Satellite altimetry observations of the Black Sea level, *J. Geophys. Res.*, *106*, 917–933, 2001.

Krivosheya, V. G., F. Nyffeler, V. G. Yakubenko, I. M. Ovchinnikov, R. D. Kosyan and E. A. Kontar, Experimental studies of eddy structures within the Rim cyclonic current zone in the north-eastern part of the Black Sea, in *Ecosystem Modeling as a Management Tool for the Black Sea*, vol. 2, edited by L. Ivanov and T. Oguz, pp. 131–144, Kluwer Acad., Norwell, Mass., 1998.

Oguz, T., and S. Besiktepe, Observations on the Rim Current structure, CIW formation and transport in the western Black Sea, *Deep Sea Res., Part I*, *46*, 1733–1753, 1999.

Oguz, T., P. La Violette, and U. Unluata, Upper layer circulation of the southern Black Sea: Its variability as inferred from hydrographic and satellite observations, *J. Geophys. Res.*, *97*, 12,569–12,584, 1992.

Oguz, T., V. S. Latun, M. A. Latif, V. V. Vladimirov, H. I. Sur, A. A. Makarov, E. Ozsoy, B. B. Kotovshchikov, V. Eremeev, and U. Unluata, Circulation in the surface and intermediate layers of the Black Sea, *Deep Sea Res., Part I*, *40*, 1597–1612, 1993.

Oguz, T., et al., Mesoscale circulation and thermohaline structure of the Black sea observed during HydroBlack'91, *Deep Sea Res., Part I*, *41*, 603–628, 1994.

Oguz, T., D. Ashwini, and P. Malanotte-Rizzoli, On the role of mesoscale processes controlling biological variability in the Black Sea: Inferrences from SeaWiFS-derived surface chlorophyll field, *Cont. Shelf. Res.*, *22*, 1477–1492, 2002.

Simonov, A. I., and E. N. Altman, *Gidrometeorologia I Gidrokhimiya Mareij SSSR*, vol. 1, *Chernoe More*, 453 pp., Hydrometeoizdat, Sevastopol, Ukraine, 1991.

Smedstad, O. M., and D. N. Fox, Assimilation of altimeter data in a two-layer primitive equation model of the Gulf Stream, *J. Phys. Oceanogr.*, *26*, 179–241, 1994.

Sokolova, E., E. V. Stanev, V. Yakubenko, I. Ovchinnikov, and R. Kosyan, Synoptic variability in the Black Sea: Analysis of hydrographic survey and altimeter data, *J. Mar. Syst.*, *31*, 45–63, 2001.

Stanev, E. V., and J. V. Staneva, The sensitivity of the heat exchange at sea surface to meso and sub-basin scale eddies: Model study for the Black Sea, *Dyn. Atmos. Oceans*, *33*, 163–189, 2001.

Stanev, E. V., P. Y. Le Traon, and E. L. Peneva, Sea level variations and their dependency on meteorological and hydrological forcing: Analysis of altimeter and surface data for the Black Sea, *J. Geophys. Res.*, *105*, 17,203–17,221, 2000.

Staneva, J. V., D. E. Dietrich, E. V. Stanev, and M. J. Bowman, Rim Current and coastal eddy mechanisms in an eddy-resolving Black Sea general circulation model, *J. Mar. Syst.*, *31*, 137–157, 2001.

Sur, H. I., E. Ozsoy, and U. Unluata, Boundary current instabilities, upwelling, shelf mixing and eutrophication processes in the Black Sea, *Prog. Oceanogr.*, *33*, 249–302, 1994.

Sur, H. I., E. Ozsoy, Y. P. Ilyin, and U. Unluata, Coastal/deep ocean interactions in the Black Sea and their ecological/environmental impacts, *J. Mar. Syst.*, *7*, 293–320, 1996.

Weaver, A. T., and D. L. Anderson, Variational assimilation of altimeter data in a multiplayer model of the tropical Pacific Ocean, *J. Phys. Oceanogr.*, *27*, 664–682, 1997.

C. Koblinsky, NASA Goddard Space Flight Center, Greenbelt, MD 20771, USA.

G. Korotaev and A. Nikiforov, Marine Hydrophysical Institute, National Academy of Sciences of Ukraine, 2 Kapitanskaya Street, Sevastopol 225000, Crimea, Ukraine.

T. Oguz, Institute of Marine Sciences, Middle East Technical University, PO Box 28, 33731, Erdemli, Mersin, Turkey. (oguz@ims.metu.edu.tr)

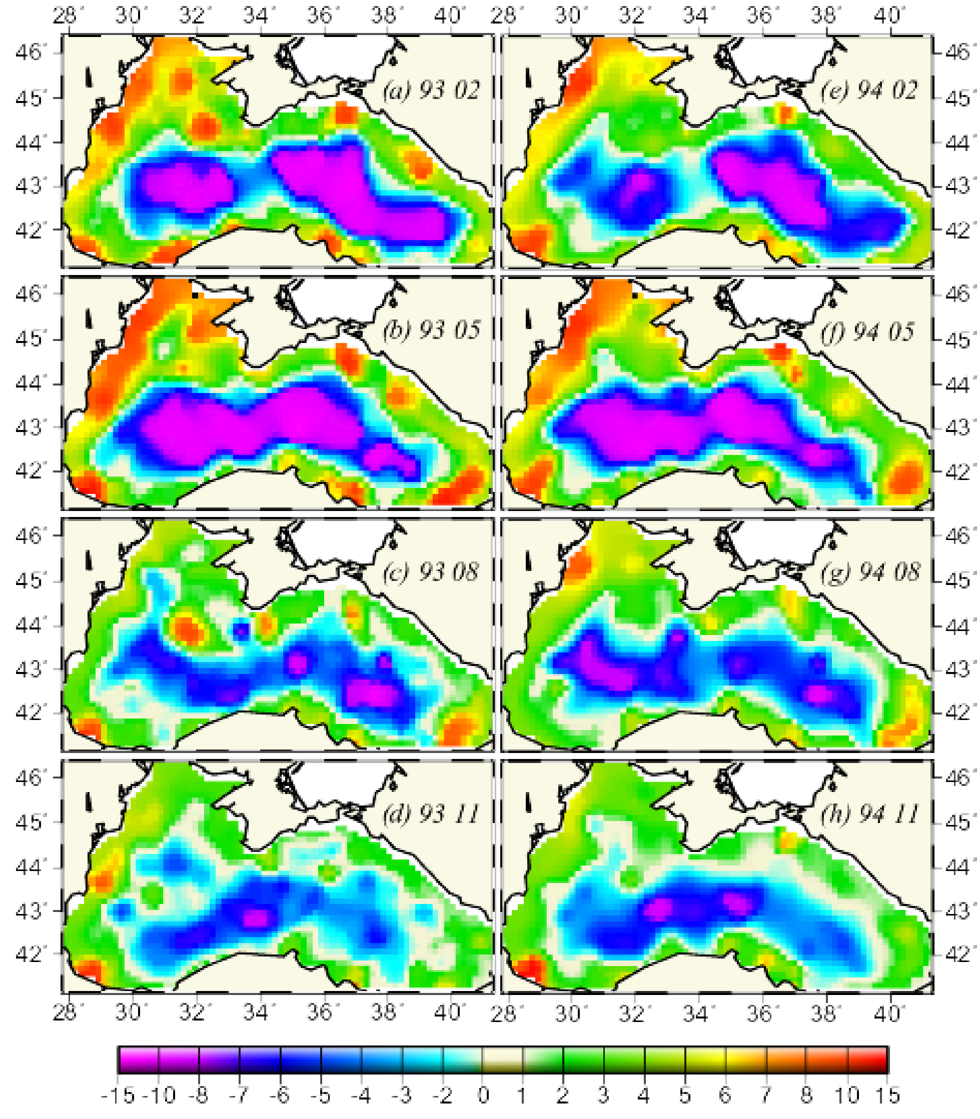

Figure 5. DSL anomaly maps (in cm) derived from assimilation of altimeter data into the model for the years (left) 1993 and (right) 1994 during (a) and (e) mid-February, (b) and (f) mid-May, (c) and (g) mid-August, and (d) and (h) mid-November.